Structural Evolution of Photoexcited Methylcobalamin Towards a CarH-like Metastable State: Evidence from Time-Resolved X-ray Absorption and X-ray Emission.

Roseanne J. Sension,[1,2,*] Taylor P. McClain,[3] Lindsay B. Michocki,[1] Nicholas A. Miller,[1] Roberto Alonso-Mori,[4] Frederico Alves Lima,[5] Fernando Ardana-Lamas,[5] Mykola Biednov,[5] Taewon Chung,[1] Aniruddha Deb,[1] Yifeng Jiang,[5] April K. Kaneshiro,[6] Dmitry Khakhulin,[5] Kevin J. Kubarych,[1] Ryan M. Lamb,[1] Joseph H. Meadows,[1] Florian Otte,[5] Danielle L. Sofferman,[7] Sanghoon Song,[4] Yohei Uemura,[5] Tim B. van Driel,[4] James E. Penner-Hahn[1,3,*]

[1]Department of Chemistry, University of Michigan, 930 N University Ave. Ann Arbor, Michigan, 48109-1055, U.S.A.

[2]Department of Physics, University of Michigan, 450 Church Street, Ann Arbor, Michigan, 48109, U.S.A.

[3]Biophysics, University of Michigan, 930 N University Ave. Ann Arbor, Michigan, 48109-1055, U.S.A.

[4]Linac Coherent Light Source, SLAC National Accelerator Laboratory, 2575 Sand Hill Road, Menlo Park, CA 94025, U.S.A.

[5]Femtosecond X-ray Experiments Group, European XFEL, Holzkoppel 4, 22869 Schenefeld, Germany

[6]Department of Biological Chemistry, 1150 W. Medical Center Dr., Ann Arbor, Michigan, 48109, U.S.A.

[7]Program in Applied Physics, University of Michigan, 450 Church Street, Ann Arbor, Michigan, 48109-1040, U.S.A.

*Corresponding Author e-mail: rsension@umich.edu, Phone: 734-763-6074; jeph@umich.edu

ABSTRACT

CarH is a protein photoreceptor that uses a form of B_{12}, adenosylcobalamin (AdoCbl), to sense light via formation of a metastable excited state. Aside from AdoCbl bound to CarH, methylcobalamin (MeCbl) is the only other example – to date – of photoexcited cobalamins forming metastable excited states with lifetimes of nanoseconds or longer. The UV-visible spectra of the excited states of MeCbl and AdoCbl bound to CarH are similar. We have used transient Co K-edge X-ray absorption and X-ray emission spectroscopies in conjunction with transient absorption spectroscopy in the UV−visible region to characterize the excited states of MeCbl. These data show that the metastable excited state of MeCbl has a slightly expanded corrin ring and increased electron density on the cobalt, but only small changes in the axial bond lengths.

TOC Graphic:

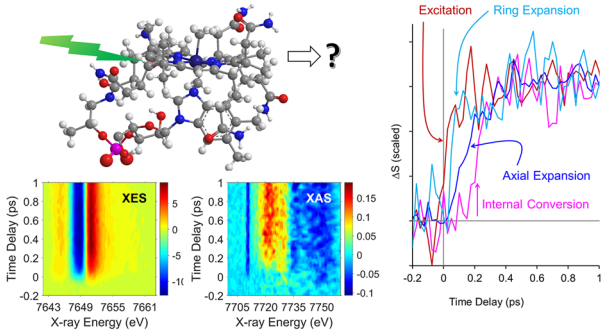

INTRODUCTION

Cobalamins perform diverse biological functions ranging from catalysis of radical rearrangement or methyl transfer in mammals[1] to the regulation of gene expression in bacteria.[2] In cobalamins, the six-coordinate cobalt is equatorially coordinated to 4 nitrogen atoms from the corrin ring, with axially coordination by a "lower" or α ligand, often dimethylbenzamidazole, and an "upper" or β ligand that varies. In methylcobalamin (MeCbl, see Figure 1) the upper ligand is a methyl group. MeCbl is one of two biologically active cobalamins, facilitating methyl transfer in mammalian enzymes including human methionine synthase.[1,3,4] Coenzyme B_{12}, where the upper ligand is a 5'-deoxyadenosyl group (AdoCbl), catalyzes radical rearrangement reaction in a variety of enzymes, including the human enzyme methylmalonyl CoA mutase.[1,4] While these enzymatic reactions involve thermal chemistry, gene regulation exploits photochemistry.[2,5] Most notably, CarH uses the photochemistry of AdoCbl to regulate carotenoid production. In addition, photoactivated cobalamins (Cbls) provide the opportunity to exert spatial and temporal control over such varied processes as drug-delivery and B_{12} bioavailability[6-9] and have attracted interest of late based on their potential as photocatalysts in synthetic chemistry.[10,11]

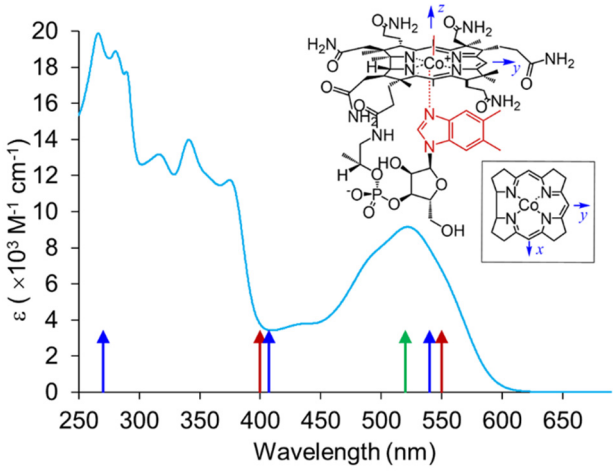

Figure 1. UV-visible absorption spectrum of MeCbl at pH 7. The vertical lines indicate the center

wavelength for pulses used to excited the MeCbl samples for UV-visible transient absorption (blue, 270 nm, 407 nm, and 540 nm), X-ray emission (red, 400 nm and 550 nm) and X-ray absorption (green, 520 nm). The inset provides a schematic diagram of MeCbl with the axis system used in our work.

Like ground state reactivity, the photochemical pathways in cobalamins are influenced both by axial ligation and by environment.[12-21] Of particular note, the initial photochemical dynamics of AdoCbl differ in water,[22] in ethylene glycol,[23,24] when bound to glutamate mutase,[18,19] and when bound to the photoreceptor, CarH.[17,21,25] The initial photochemical dynamics observed for AdoCbl bound to CarH are characterized by formation of a long-lived excited state prior to bond cleavage. The dynamics and the excited state optical spectrum resemble more closely those of MeCbl in water than those of AdoCbl in water, ethylene glycol or bound to the enzyme glutamate mutase.[17,21] Aside from CarH, MeCbl is the only other example – to date – of a photoexcited cobalamin forming a metastable excited state with a lifetime of nanoseconds or longer.

Time-resolved X-ray spectroscopies provide the opportunity to characterize excited state structure and dynamics with a level of precision and detail inaccessible by other methods. While direct measurements on CarH are complicated by limited quantities and low concentrations, MeCbl is readily available and samples can be prepared in mM concentration. In order to better understand the nature of the unique, long-lived excited states that are formed in CarH and MeCbl, we have used a combination of ultrafast optical and X-ray spectroscopies (polarized X-ray absorption near edge structure (XANES) measurements and time-resolved X-ray emission spectra (XES) in the Co $K\alpha_{1,2}$, $K\beta_{1,3}$, and valence-to-core (VtC) regions) to probe the initial dynamics of MeCbl in water following optical excitation.

EXPERIMENTAL METHODS

Methylcobalamin was purchased from MilliporeSigma and used as received. Solutions were prepared by dissolving methylcobalamin in deionized water to produce ~0.6 mM solutions for UV-visible measurements and ~4 to 8 mM solutions for X-ray absorption and X-ray emission measurements. Sample preparation took place under red light to avoid photolysis. Solutions for UV-visible measurements were deoxygenated by bubbling nitrogen for at least an hour and maintained under a positive pressure of nitrogen during measurements. The sample was circulated through a fused silica flow cell with an optical path length of 1 mm to refresh the sample between laser pulses. For XANES measurements, the samples were filtered, centrifuged, and pumped through a glass nozzle to achieve a stable 50 μm diameter jet of solution. For XES measurements, the sample was delivered as a 100 μm thick cylindrical jet running with a linear speed of about 60 m/s. Samples were monitored using UV-visible absorption to ensure that any buildup of photoproducts remained insignificant.

UV-Visible Transient Absorption. UV-visible TA spectra of MeCbl were obtained using a 1 kHz Ti:sapphire laser system producing ca. 70 fs compressed pulses centered around 814 nm. Pump pulses were generated by frequency doubling the fundamental in a β-barium borate crystal to ca. 407 nm, summing 407 nm and 814 nm to produce 270 nm pulses, or pumping a noncollinear optical parametric amplifier to generate 540 nm pulses. A portion of the 407 nm beam was used to produce a broadband continuum probe in a translating CaF_2 window, spanning the range from 290 nm to 600 nm. Alternatively, the 814 nm fundamental was used to produce a broadband continuum probe spanning the range from 320 nm to 750 nm. All measurements were performed with the polarization of the pump and probe pulses at magic angle (54.7°) with respect to each other. These measurements characterize the spectral evolution out to hundreds of picoseconds

complementing our earlier measurements which were only performed at specific wavelengths or select time delays.[26-29]

X-ray Absorption Near Edge Structure (XANES) Measurements. Time-resolved polarized XANES measurements of MeCbl were performed using the XPP instrument of the x-ray free electron laser LCLS at SLAC[30] using the liquid jet endstation.[31] The X-ray beam and laser beam travel in a nearly collinear geometry (~1° crossing angle) and were overlapped with the sample about 500 μm from the nozzle producing the sample jet. The optical pump pulse was 520 nm, ~50 fs FWHM and the X-ray probe pulse (~50 fs) was scanned from 7.7 to 7.76 keV. Cobalt X-ray fluorescence was collected and used as a measure of X-ray absorption where the signal was normalized to the small-angle scattering from the solvent. Both the optical and X-ray pulses were linearly polarized. A waveplate in the optical beam was used to rotate the polarization to acquire transient spectra with the polarization of the optical pulse parallel and perpendicular to the X-ray pulses. The excitation fraction of ~0.25 was estimated as described previously.[32] The XANES spectrum of ground state MeCbl was also obtained at SSRL beamline 9-3 for intensity scaling of the simulated and experimental spectra. The synchrotron data were measured on frozen solutions at ~10K as fluorescence excitation spectra, detected with a 100-element solid-state Ge detector array with an Fe filter and Soller slits.

X-ray emission spectral (XES) Measurements. XES difference spectra of MeCbl in the Co $K\alpha_{1,2}$, Co $K\beta_{1,3}$ and valence-to-core (VtC) regions were obtained at the FXE instrument of the European X-ray free electron laser (EuXFEL).[33-35] The experiments were performed using the dedicated chamber for experiments on liquid samples.[36] The optical excitation wavelength was 550 nm or 400 nm, ~70 fs duration (FWHM), with a laser/X-ray crossing angle of ca. 2°. The sample concentration was ~4 mM with 400 nm excitation and ~8 mM with 550 nm excitation. The

sample integrity throughout each run was confirmed by UV-Vis spectroscopy. The incident X-ray energy of the pulses was set to 9.3 keV and the intra-train repetition rate was either 0.564 or 0.282 MHz. Emission spectra were measured with a dispersive X-ray spectrometer operating in the von Hamos geometry and equipped with 7-10 Ge(111) analyzers at ~83 degrees for measuring the Co Kβ and 5-8 Si(531) analyzers at ~77 degrees for the Co Kα over two experimental campaigns. All cylindrical analyzers have 500 mm radius of curvature. The Co Kα and Kβ signals were recorded simultaneously using two distinct detectors, namely a Jungfrau 1M and a 500K, respectively. The von Hamos spectrometer has a limited dispersion window in the Co Kβ region and did not allow detecting the complete $K\beta_{1,3}$ and VtC at once. Measurements of the VtC region were performed by slightly changing the Bragg angle on the Ge(111) analyzers and moving the Jungfrau detector accordingly. Both Jungfrau detectors integrated all pulses (total 140 for the experiments using 550 nm excitation or 200 for the experiment using 400 nm excitation) in each train from the European XFEL burst mode operation. The pump-probe signal was generated by pumping every second train (5 Hz) and the differences are constructed by first integrating all of pump-on and all of the pump-off trains for a given delay time, normalizing each of these to the total integrated Kα or Kβ intensity and then subtracting the normalized pump-off from the normalized pump-on signal.

Computational Methods. The Finite Difference Method Near Edge Structure (FDMNES) program was used to simulate the ground and excited state XANES spectra as a function of molecular structure.[37,38] For most FDMNES simulations the cobalamin structure was truncated by removing the tail and replacing the peripheral groups on the corrin ring with methyl groups. The quantum chemical package Orca 4.2.1[39,40] was used to perform time-dependent density functional theory (TD-DFT) calculations with the B3LYP functional, ZORA-def2-TZVP basis, and CPCM solvent to model the pre-edge region of the ground state spectra of MeCbl as well as the ground

state valence-to-core emission spectrum. These calculations were performed on a truncated structure replacing the peripheral groups on the corrin ring with hydrogen. Some calculations were performed without the CPCM solvent model and the resulting spectra are nearly identical to those presented here.

Optical transient absorption measurements, XANES pre-edge, and time-resolved XES measurements were fit to a model consisting of a sum of exponential decay components using the global analysis program Glotaran.[41]

RESULTS

UV-Visible absorption shows 4 distinct excited state species

Broadband UV-visible transient absorption measurements of MeCbl following 540 nm excitation were performed to refine the results from earlier single wavelength measurements and to better characterize the spectra of the intermediate species.[26-29] The experimental results were fit to a sum of exponential decay components, with four distinct excited state species (labeled **A** to **D)** prior to bond homolysis or ground state recovery. The results are summarized in Figure 2 and in a contour plot in Figure S1. The new measurements identify an initial component, τ_A = 130 fs, not observable in the original experiments. The spectrum of this initial species is dominated by bleaching of the visible absorption band, a signature consistent with stimulated emission to the red of the ground state absorption, and the appearance of a broad excited state absorption. The spectra of the next three excited state species are similar to each other. In the visible region, the difference spectra exhibit relatively small changes from the ground state spectrum and all three species show the appearance of a prominent band at 340 nm, consistent with the earlier measurements.[17,27] The decay of the second species, **B** ($\tau_B \approx 1.7$ ps), is in good agreement with the 1.5 ± 0.5 ps component identified earlier.[26] This component makes the largest contribution to the difference spectrum

between 540 nm and 600 nm. The lifetime of **C** (τ_C = 28 ps), is longer than the 17 ± 0.5 ps component reported earlier.[26] This difference is a consequence of better signal-to-noise in the new measurements and of the ability to measure the broadband difference spectrum for global analysis. The influence of τ_C on the overall quality of the fit is most prominent around 430 nm – a region that was not probed in the earlier measurements. The current data set extends only to 750 ps limiting our ability to determine the lifetime of **D**, although not interfering with our ability to determine the spectrum of **D**; fortunately, **D** has been shown previously to decay on a ca. 1 ns time scale, resulting in the formation of cob(II)alamin (~15%) or return to the ground state (~85%) and these lifetimes could be used to constrain the present fits (see below).[26]

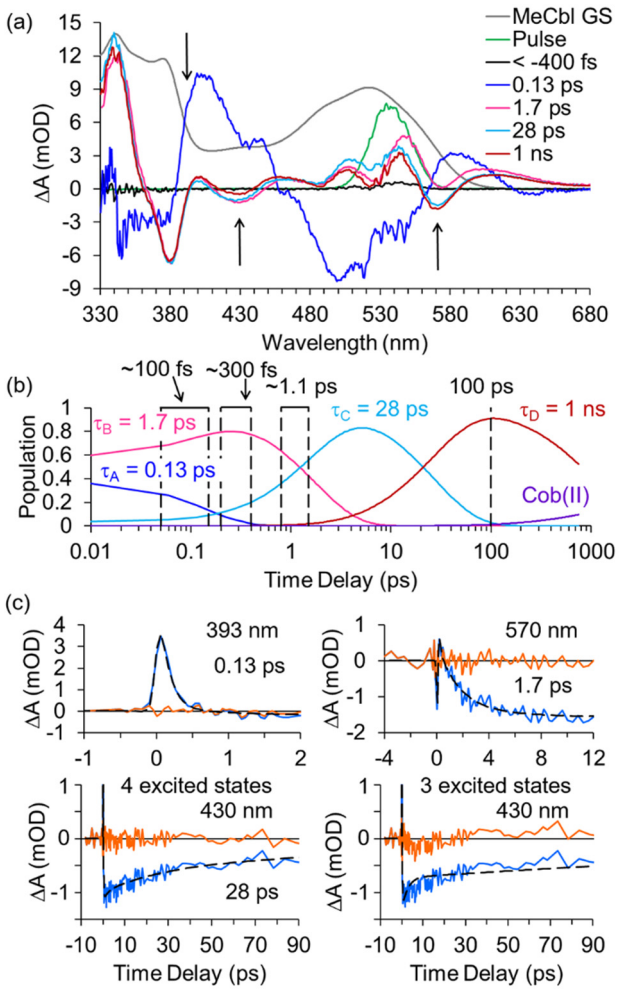

Figure 2. Optical transient absorption results following excitation of MeCbl in water (pH ~7) at 540 nm. (a). The transient spectra were fit to a sum of exponential components resulting in the evolution associated difference spectra plotted in the top panel. The difference spectra are compared with the optical pulse used to excited the sample and with the ground state spectrum of MeCbl. (b). The transient populations of the intermediate states determined from the fit to the data. The vertical dashed lines indicate the time delay ranges used for excited state XANES and XES spectra (see below). (c). Sample kinetic traces (blue) at 393 nm, 430 nm, and 570 nm, together with the best fits (black dashed lines) and residuals (orange). For 430 nm, fits are compared for models using 3 or 4 excited state species before bond homolysis, illustrating the need for four excited state species in the fit.

The excited state and product spectra can be estimated from the difference spectra in Figure 2 using:

$$A_{ES} = \left(\Delta A + A_{GS} \cdot \alpha\right) / \alpha \quad (1)$$

where α is scale factor depending on the excitation fraction, the quantum yield for excited state or product formation, and the differences in concentration and path length for the steady state absorption measurement of A_{GS} and the transient absorption measurements. The spectrum of the long-lived excited state of MeCbl reported earlier was used to constrain α.[17,27] The estimated spectrum of the initial excited state, **A**, is plotted in Figure 3 along with the difference spectra measured at the earliest times. This excited state is characterized by a broad excited state absorption. The apparent decrease in absorbance in the red, where there is no ground-state absorption, is a signature of stimulated emission.

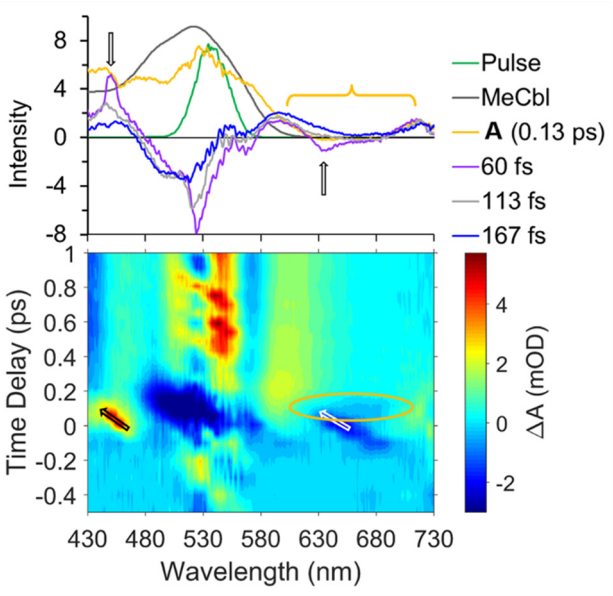

Figure 3. Time resolved difference spectra and estimated excited state UV-visible spectra for the initial excited state, **A**, following excitation of MeCbl. The arrows indicate features assigned to Stokes and anti-Stokes stimulated Raman scattering from the water solvent. The yellow bracket and oval highlight the signature of stimulated emission in the data. The left axis in the upper plot is ΔA (mOD) for the difference spectra and ε ($\times 10^3$ M^{-1} cm^{-1}) for the spectra of the ground state and **A**. The scaled intensity of the pump pulse is shown for comparison.

The estimated excited state spectra for **B**, **C**, and **D** are plotted in Figure 4. Following internal conversion from the initial excited state **A**, the subsequent excited states of MeCbl all have similar spectra, resembling the ground state spectra of typical cob(III)alamins. The transition of MeCbl from **B** to **C** ($\tau_B = 1.7$ ps) is characterized by a small increase in the peaks of the major absorption bands and a decrease in absorption on the red-wing of the visible band. The transition of MeCbl from **C** to the metastable excited state **D** ($\tau_C = 28$ ps) is characterized primarily by a small increase in absorption bands around 430 nm.

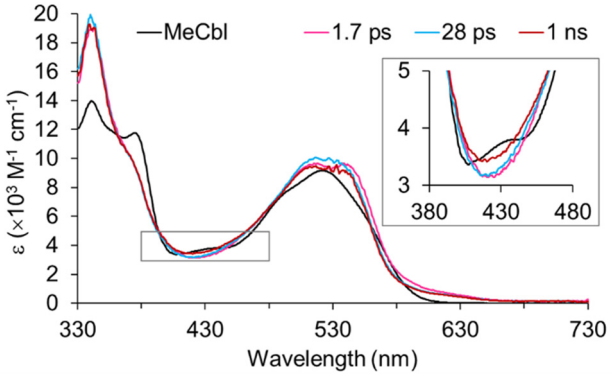

Figure 4. Estimated excited state UV-visible spectra for MeCbl. The excited states are designated by their lifetimes. The inset in the plot illustrates the primary difference between the 28 ps state **C** and the 1 ns state **D** of MeCbl. The spectrum of the short-lived species **A** is plotted in Figure 3.

Broadband UV-visible transient absorption measurements of MeCbl following 407 nm and 270 nm excitation were also performed, spanning time ranges from shortly before t=0 to 900 ps (407 nm) or 750 ps (270 nm). These measurements are consistent with the earlier measurements performed at select time delays or select wavelengths,[26-29] but provide a more comprehensive picture of the excited state dynamics. These data are discussed in greater detail in supporting information.

Adenosylcobalamin in solution is also characterized by several excited state species with distinct spectral signatures. Evolution out of the initial Franck-Condon excited state, designated **A**, occurs on a time scale of ca. 200 to 300 fs, populating a relaxed excited state, designated **B**, with a lifetime of 1.7 ps in water and 13 ps in ethylene glycol.[17,42] In both water and ethylene glycol, this is followed by evolution to an excited state, designated **C**, that is characterized by a significant decrease in intensity in the visible region of the spectrum (see Figure 5). In ethylene glycol this state decays via bond homolysis forming cob(II)alamin on a ca. 100 ps time scale, while in water an additional excited state, designated **D**, characterized by a blue-shifted spectrum is populated prior to bond dissociation on a ca. 100 ps time scale.[15,24] When AdoCbl is bound to

glutamate mutase, the excited states **B** and **C** are similar to the excited state of methylcobalamin or of AdoCbl bound to CarH, but again, bond homolysis occurs on a ca. 100 ps time scale in glutamate mutase, much faster than is seen for CarH.[15,18,19] The UV-visible transient absorption results show that MeCbl in solution is a better model than AdoCbl in solution for the excited electronic states of AdoCbl bound to CarH.

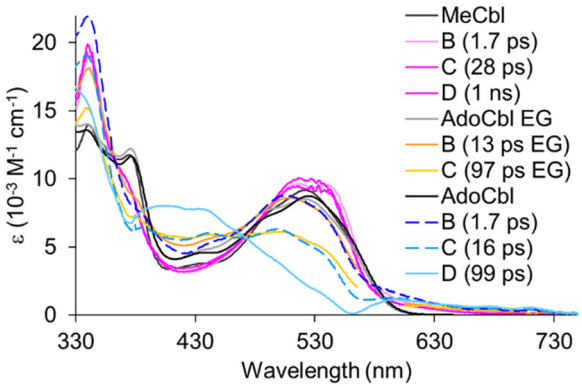

Figure 5. Comparison of the excited state spectra of MeCbl and AdoCbl. The spectra of state B for AdoCbl are adapted from Figure S5 of ref. [17]. Copyright 2020, American Chemical Society. The spectra of C and D are from the same data. The evolution of the excited state for AdoCbl in water or ethylene glycol (EG) is distinct from the evolution of MeCbl in solution or of AdoCbl bound to CarH or to glutamate mutase.[17]

Time-resolved XANES measurements show anisotropic structural changes

Polarized time-resolved XANES measurements were performed for methylcobalamin following excitation at 520 nm for time-delays from -.5 to 1.5 ps and at 100 ps. Data were obtained using parallel and perpendicular polarization with the total signal calculated as $\Delta S = \Delta S_{\parallel} + 2\Delta S_{\perp}$. The total signal obtained at early time delays following excitation of MeCbl is plotted in Figure 6.

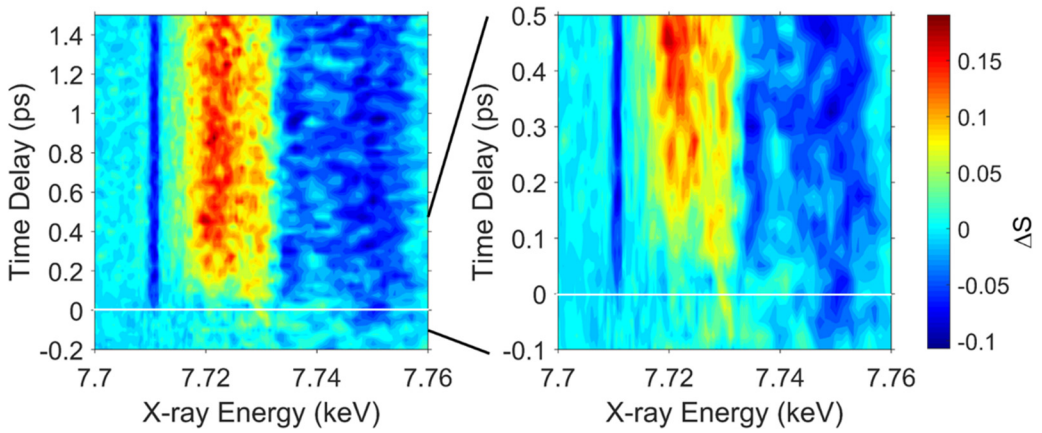

Figure 6. Isotropic XANES difference spectrum of MeCbl as a function of time delay following excitation at 520 nm. The data were oversampled along the energy axis and are smoothed using a three point running average. The plot on the right is expanded to emphasize the early time behavior.

The estimated excited state spectra are calculated from the difference spectra using:

$$S_{ES} = \frac{\Delta S_{\parallel} + 2\Delta S_{\perp}}{3} f \cdot \varphi + S_{GS} \tag{2}$$

where f is the excitation fraction and φ is the quantum yield. The excitation fraction was ~0.25[32] and φ for excited state formation is ~1 at 0.3 ps and 1.5 ps and 0.95 at 100 ps. The isotropic difference spectra are compared with the ground and estimated excited state spectra in Figure 7. The time resolved XANES results at 100 ps and the estimate of the difference spectrum for the formation of cob(II)alamin were reported previously.[32]

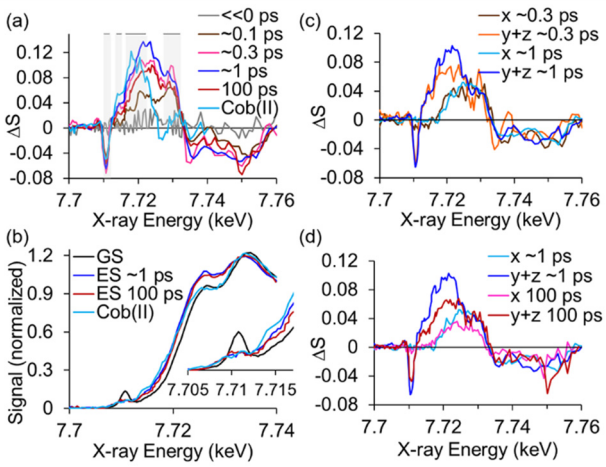

Figure 7. (a) The isotropic difference spectra for MeCbl at select time delays. The shaded regions indicate the energy regions averaged for the kinetic traces in Figure 8. (b) Ground state XANES spectrum of MeCbl (GS black) and estimated excited state spectra at the indicated time delays. The inset emphasizes the changes in the pre-edge region. The cob(II)alamin and 100 ps excited state spectra are adapted from ref.[32] copyright 2019, American Chemical Society. (c) and (d) Decomposition of the XANES difference spectra into contributions along (*x*) and perpendicular (*y*+*z*) to the transition dipole initially excited. For the time delays indicated.

Polarization decomposition of the transient XANES spectra provides more insight into the evolution of MeCbl on the excited state surface. The signals obtained with parallel and perpendicular polarization are used to separate the contributions along the transition dipole initially excited, designated "*x*", and the sum of the two perpendicular directions, "*y*+*z*".

$$\Delta S_x = 2\Delta S_{\parallel} - \Delta S_{\perp}$$
$$\Delta S_{y+z} = 3\Delta S_{\perp} - \Delta S_{\parallel} \quad (3)$$

The transition dipole lies in the corrin ring and thus ΔS_x probes equatorial changes in structure, while ΔS_{y+z} includes both equatorial and axial contributions.

The decompositions of the difference spectra for MeCbl averaged around 0.3 ps, around 1 ps, and at 100 ps are plotted in Figure 7. The time dependent polarization decomposition at three key

energies is plotted in Figure 8. The pre-edge bleach at 7.711 keV is the earliest transient observed in the data and we use this to define zero time-delay. The transients around 7.72 keV and 7.73 keV monitor the edge-shift and the initial peak amplitude, respectively. As shown in simulations (see below), the former is most sensitive to average nearest-neighbor distance, while the latter is primarily a marker of corrin ring expansion. From ~0.3 ps [**B** (~79%), **C** (~15%)] to ~1 ps [**B** (~52%), **C** (~47%)] the *x*-polarized component is unchanged within the accuracy of the measurement suggesting that much of the ring expansion occurs on time scales <300 fs. The primary change in the spectrum between 300 fs and 1 ps is an increase in the intensity of the *y*+*z* polarized signal around 7.72 keV suggesting that out of plane motions of the ring or the axial ligands occur on this picosecond time scale. The 100 ps spectrum [**D** (95%)] is characterized by a decrease in the ring expansion as shown by the decrease in the edge-shift.

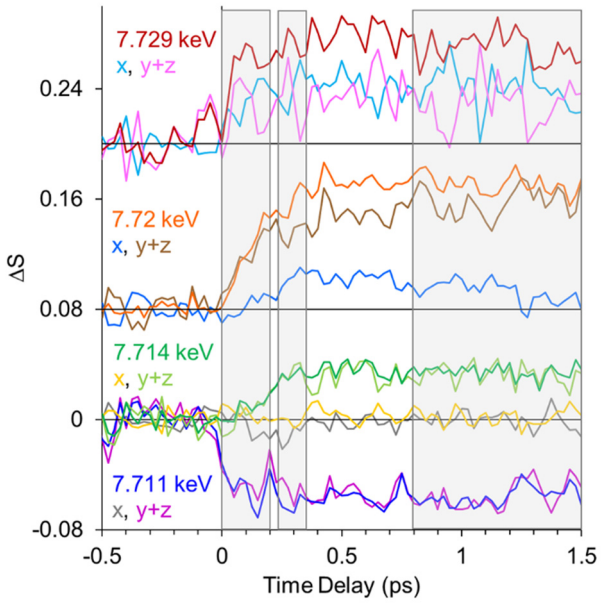

Figure 8. Decomposition of the transient XANES signal at key energies following excitation of MeCbl. The bleach of the pre-edge transition at 7.711 keV is prompt and contains little or no contribution from the x-direction. This is consistent with a bleaching of a *z*-polarized 1*s*→3*d* transition. The signal at 7.714 keV reflects the delayed appearance of a *y*- or *z*-polarized excited

state 1*s* to ligand pre-edge transition. The signal at 7.73 keV appears quickly and contains approximately equal contributions from the *x* and *y*+*z* directions, while the signal monitoring the edge-shift at 7.72 keV is dominated by the *y*+*z* contribution and appears later. The shaded regions indicate the time windows averaged for Figure 7.

Time-resolved XES measurements show changes in electronic structure

Time-resolved X-ray emission measurements were performed at the FXE instrument at the European XFEL for MeCbl following photoexcitation at 400 nm or 550 nm. The incident X-ray energy was 9.3 keV and the detection range covered the $K\alpha_{1,2}$, $K\beta_{1,3}$, and valence-to-core regions. Time-resolved XES measurements following excitation at 550 nm are plotted in Figure 9. Time zero for these measurements is defined by the transient averaged around 7.645 keV as this is the earliest transient identified in the data. The difference spectra obtained for time delays averaged from 0.05 ps to 0.15 ps (~100 fs), 0.2 ps to 0.4 ps (~300 fs), 0.8 ps to 1.5 ps (~1 ps), and at 100 ps are plotted in Figure 10(b). XAS difference spectra averaged over similar time ranges are shown for comparison in Figure 7(a). All of the XES transients in the $K\beta_{1,3}$ region show a blue-shift in the peak of the emission band and an increase in the splitting of the transitions underlying the observed band, resulting in an overall increase in bandwidth and a characteristic up-down-up difference signal. The XES difference is slightly larger at 300 fs spectrum than at 1 ps, in contrast to the structural evolution probed by XANES, which increases from 300 fs to 1 ps. The XES peak width decreases slightly from 1 to 100 ps, but remains significantly larger than in the ground state.

The difference signal in the valence-to-core region also evolves between 50 fs and 1 ps reaching a maximum depletion of emission around 300 fs followed by a slight recovery of intensity accompanied by a red-shift of the peak of the difference signal by ~0.2 eV. In the long-lived excited state probed at 100 ps, the intensity of emission in the valence-to-core region has recovered further, accompanied by a change in the shape of the difference signal. These changes reflect an evolution

in the electronic configuration and/or corrin ring structure between 1 ps (**B**) and 100 ps (**D**).

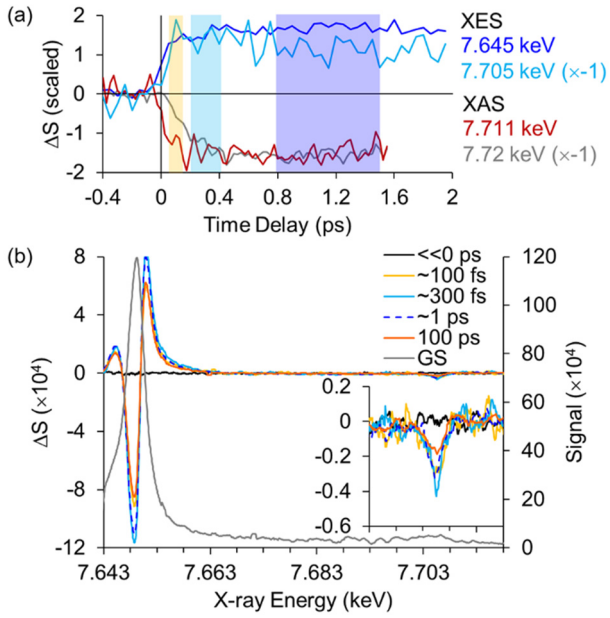

Figure 9. Time-resolved X-ray emission spectra for MeCbl. (a) The top panel illustrates the time dependence for the signals averaged around 7.645 keV (Kβ XES) and 7.109 keV (1s-3d XAS) used to define time zero in the XES and XAS spectra respectively. The rise of the tr-XAS signal at 7.72 keV and the XES signal integrated over the valence-to-core (~7.703.5 - 7.706.5 keV) are also plotted. The shaded boxes indicate the regions averaged for the plots in (b). (b) The XES difference spectra over indicated time ranges. The total emission signal is normalized to an integrated area of 1, and multiplied by 10^4 for plotting. The ~1 ps spectrum is dashed to avoid obscuring the ~300 fs spectrum. The difference spectra in the valence-to-core region are shown on an expanded scale in the inset.

The transient XES in the $K\alpha_{1,2}$, $K\beta_{1,3}$, and valence-to-core regions were fit to a sum of exponential decay components using the time constants obtained from analysis of the UV-visible transient absorption spectra. Species associated difference spectra for the species **A**, **B**, and **C** are obtained from this analysis. The difference spectrum corresponding to species **D** is obtained from the measurement at 100 ps. These difference spectra are plotted in Figure 10. Plots illustrating the

quality of the fit are included in Figures S3-S5. The initial difference spectrum following photoexcitation (**A**, τ=0.13 ps) is symmetric, suggesting a broadening of the Kα and Kβ mainline emission peaks as the main effect on this time scale accompanied by a decrease in the VtC emission peaking at 7706.1 eV. The spectrum of **B** (τ=1.7 ps) exhibits the most significant deviation from the ground state spectrum, characterized by a blue-shift of the $K\beta_{1,3}$ mainline peak and a decrease in the VtC emission intensity and a shift in the VtC minimum to 7705.7 eV. The tr-XES difference spectra of **C** (τ=28 ps) and **D** (τ=1 ns) are similar in magnitude and shape characterized by a decrease in the blue shift of the Kβ mainline peak. For **D** the VtC difference decreases in amplitude and shifts to lower energy.

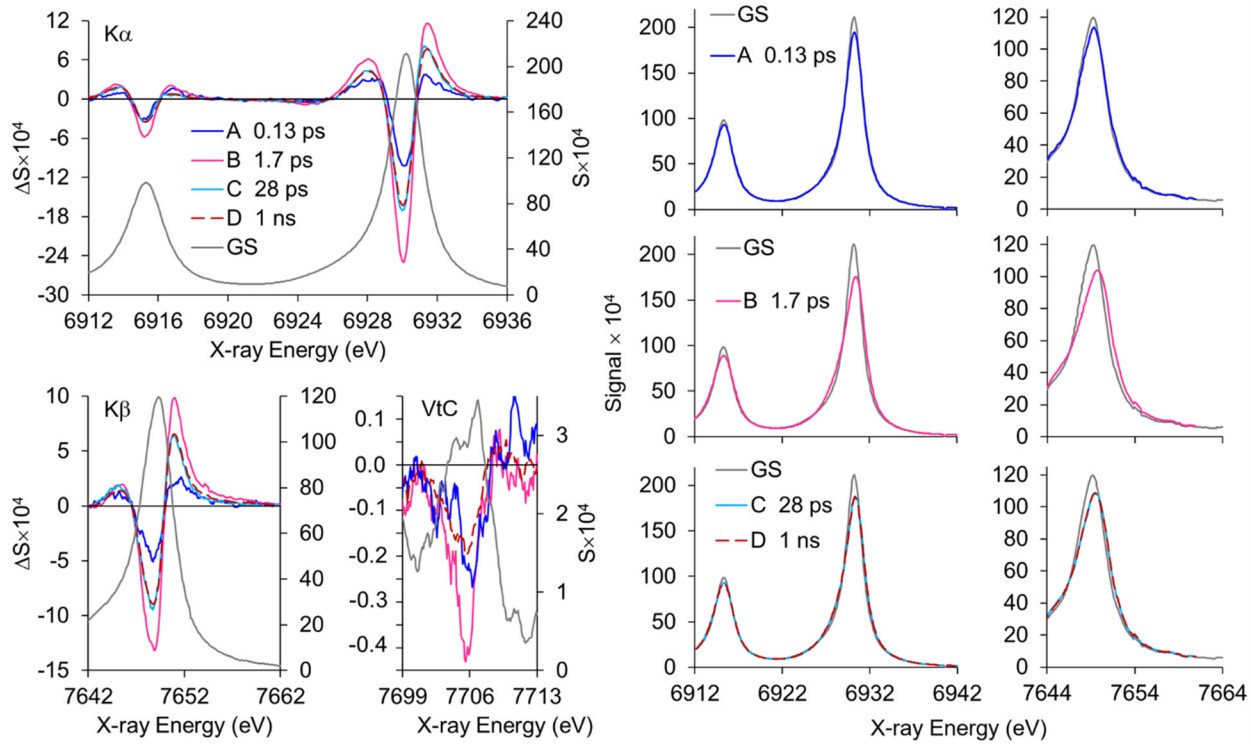

Figure 10. Left: Evolution associated difference spectra obtained from a fit to the transient XES spectra. The upper panel illustrates the spectra in the $K\alpha_{1,2}$ region while the lower panel contains the $K\beta_{1,3}$ region and the valence-to-core region. In the VtC region, the difference spectrum for **C** is complicated by the low signal and the fact that the traces only cover time delays out to 2 ps and is

not plotted. The left axis label ($\Delta S \times 10^4$) and right axis label ($S \times 10^4$) apply to both Kβ and VtC. Right: Estimated excited state XES spectra in the Kα and Kβ mainline regions of the spectrum for an excitation fraction of $f = 0.6$.

The excited state spectra can be estimated from the evolution associated difference spectra assuming an excitation fraction. For the XES measurements the excitation fraction is estimated to be $f = 0.6 \pm 0.1$, although a larger value is possible. The general trends are similar for any excitation fraction between 0.5 and 1. Fractions <~0.45 produce estimated spectra having unrealistic shapes for one or more of the peaks. The excited state **B** exhibits a pronounced blue-shift of the $K\alpha_1$ and Kβ mainline peaks, while **C** and **D** have a smaller blue-shift.

Time-resolved X-ray emission measurements were also performed at the FXE instrument for MeCbl following photoexcitation at 400 nm. The incident X-ray energy was 9.3 keV and the detection range covered the $K\alpha_{1,2}$, $K\beta_{1,3}$, and Kβ′ regions. The difference spectra obtained at four key time delays are summarized in Figure 11. Given a branching of 3:1 between formation of the metastable excited state and prompt dissociation to cob(II)alamin and a 1 ns lifetime for the metastable excited state, the data obtained at ca. 15 ps and at 1 ns can be used to estimate difference spectra for the excited state and for the formation of cob(II)alamin. These are plotted in Figure 11(b). The difference spectra of the excited state species (**D**) are similar for both excitation wavelengths. These are distinct from the difference spectrum for the formation of cob(II)alamin from MeCbl. The latter has a shape that is consistent with that observed for dissociation of AdoCbl using 550 nm excitation pulses. Formation of cob(II)alamin results in a broadening of the $K\beta_{1,3}$ transition, while formation of the electronic excited state of MeCbl results in a clear blue-shift of this transition. It is also clear that the differences in the Kβ′ region for the formation of cob(II)alamin are no larger than the differences for population of the excited electronic state and

may even be somewhat smaller. Analogous, albeit much smaller, distinctions between the spectra for **D** and those for Co(II)alamin may also be present in the Kα region.

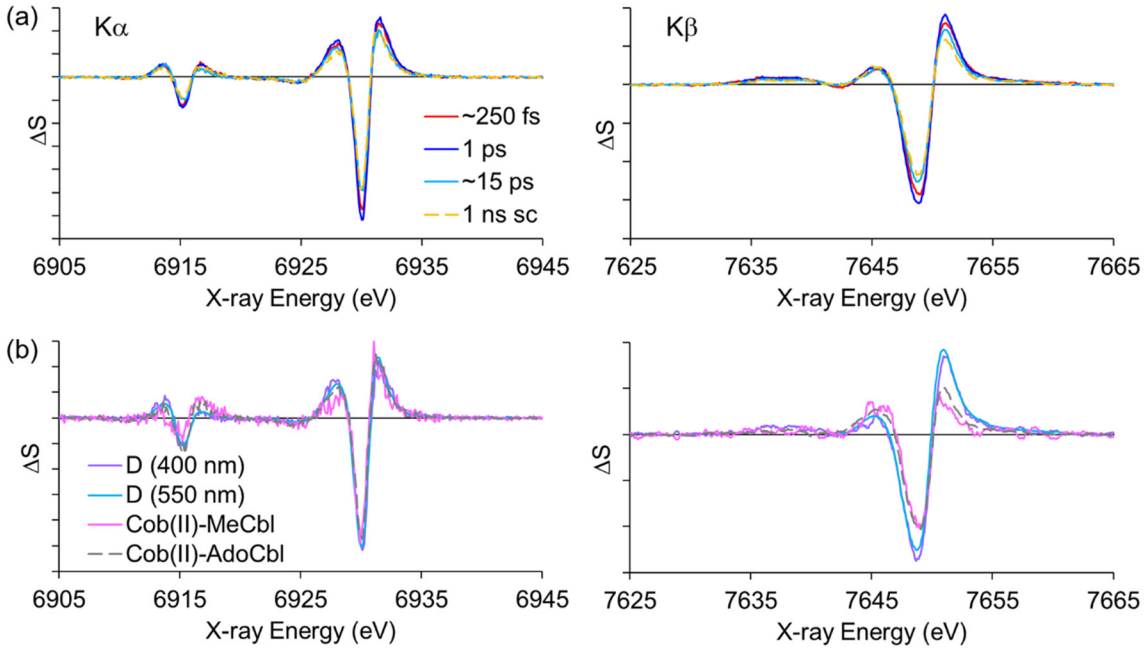

Figure 11. (a) Difference spectra obtained at the indicated time delays following excitation of MeCbl at 400 nm. The spectrum at ~250 fs represents an average from 100 fs to 400 fs and the spectrum at ~15 ps represents an average of data from 10 to 20 ps. The legend is the same for the Kα and Kβ regions. The 1 ns spectrum is scaled to account for the quantum yield for ground state recovery at 1 ns. (b) Decomposition of the difference spectra following excitation at 400 nm into contributions from the metastable excited state **D** and the formation of cob(II)alamin following bond dissociation. The difference spectrum corresponding to population of the metastable excited state is compared with the spectrum obtained following 550 nm excitation and the difference spectrum corresponding to bond dissociation is compared with the difference spectrum for dissociation of AdoCbl to form cob(II)alamin 450 ps after excitation at 550 nm.

XANES simulations characterize corrin dynamics

In our earlier paper we used FDMNES[37,38] simulations to model the long-lived excited state of MeCbl probed 100 ps after excitation.[32] Simulations were performed starting with the truncated

structures for the ground and excited states optimized by Lodowski et al. using DFT and TD-DFT methods.[43] The primary conclusions from that study were: (1) The dominant contribution to the difference between the ground and excited state is an expansion and distortion of the corrin ring. (2) The experimental XANES difference spectrum requires a larger distortion or expansion of the corrin ring than is predicted using TD-DFT. This was modeled by using the crystal structure for the adenosylrhodibalamin (AdoRbl) ring where a Rh^{3+} ion replaces the Co^{3+} in cobalamins.[44] (3) The large 0.12 Å contraction of the Co-N_{IM} distance predicted by Lodowski et al. was not consistent with the data although a contraction of ≤0.05 Å was deemed possible.

In the analysis reported here, we use a larger model system with methyl groups rather than hydrogen atoms replacing the peripheral groups on the ring, a benzimidazole rather than imidazole for the lower axial ligand, and we begin with the corrin ring structure obtained from the crystal structure of ethylcobalamin reported by Hannibal et al.[45] rather than the DFT optimized corrin ring. A Co-C bond length of ca. 2.000 ± 0.025 Å and a Co-N_{DMB} bond length of 2.23 ± 0.01 Å results in a simulated XANES spectrum in good agreement with the measured spectrum as discussed in detail elsewhere.[46] This structure was used as a starting point for exploring the structural dynamics in the excited state.

In agreement with our earlier results, an expansion of the corrin ring is required to account for the magnitude of the *x*-polarized component of the transient XANES difference spectrum at 100 ps. This ring expansion is consistent with about 70% of the difference between the ground state and Rbl rings as illustrated in Figure 12(d). The average increase in the equatorial Co-N bonds in the simulation is +0.058 Å (range: +0.050 Å to +0.066 Å). The ring expansion may be accompanied by relatively small expansions (≤0.05 Å) of one or both axial bonds, although the large number of potential distortions of the corrin ring make it difficult to be certain. It is possible

that the difference signal is due entirely to changes in the structure of the corrin ring in the excited state, without significant change in the axial bond distances. Our earlier conclusion that a small (<0.05 Å) contraction of the Co-N_{DMB} bond might be possible is not consistent with the current simulations using a larger molecule and starting with crystal structures rather than DFT predictions for the ring unless it is compensated by some distortion of the corrin ring. The calculations do not predict such a distortion.

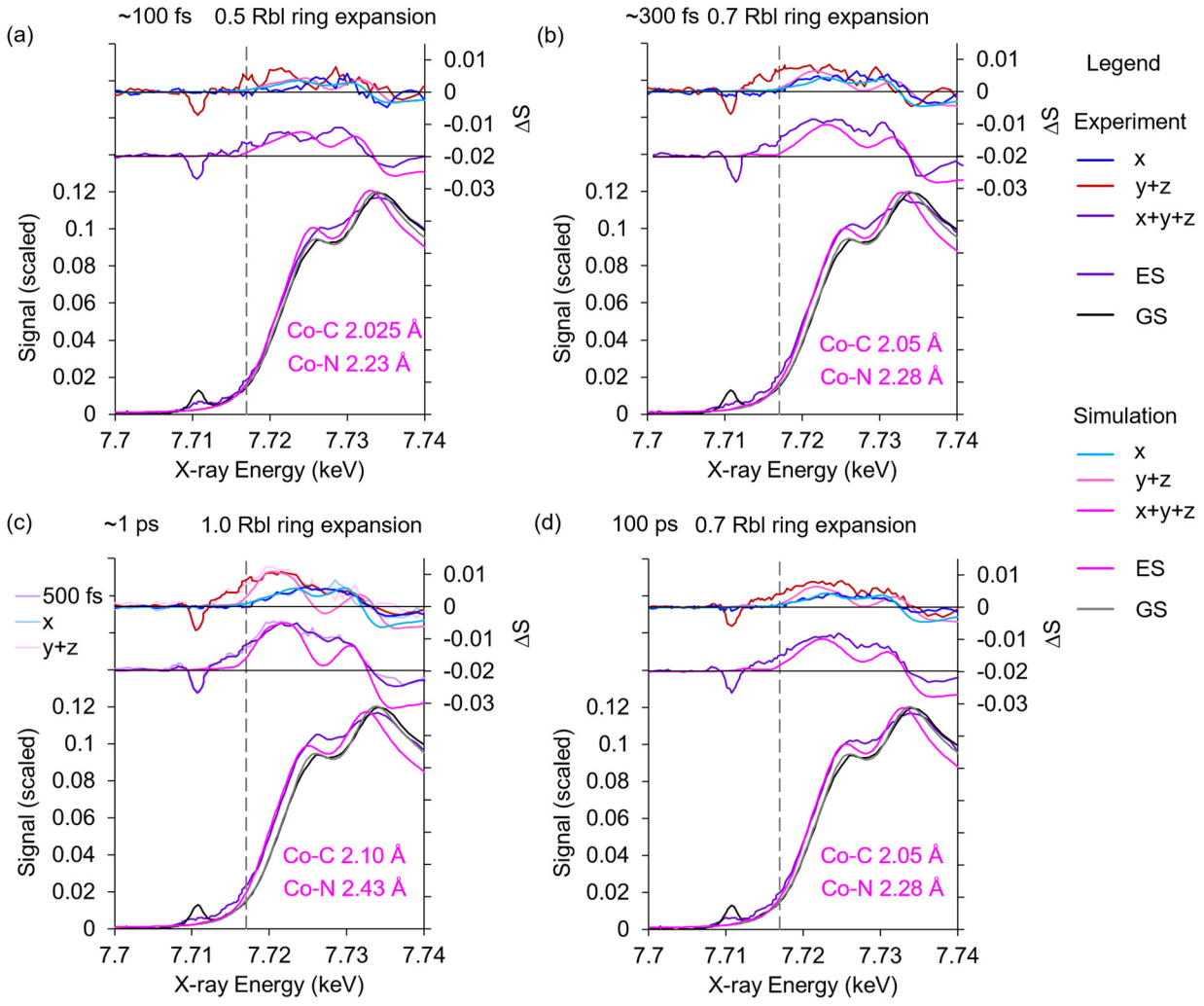

Figure 12. Comparison of experimental difference spectra and estimated excited state spectra for MeCbl with simulated spectra. In each panel the black line is the experimental ground state spectrum and the gray line is the simulated spectrum as described above. The vertical dashed line is the

approximate break between the pre-edge and XANES regions. (a) The difference spectrum and estimated excited state spectrum at ~100 fs compared with the simulated results using ground state axial bond lengths and an expanded ring 50% of the distance between the ground state ring and the Rbl ring. (b) The difference spectrum and estimated excited state spectrum at ~300 fs compared with the simulated results using ground state axial bond lengths and a corrin ring expanded 70% of the distance between the ground state ring and the Rbl ring and the axial bonds expanded by 0.05 Å. (c) The difference spectrum and estimated excited state spectrum at ~1 ps compared with the simulated results using an expanded ring obtained from the crystal structure of Rbl and axial bonds expanded by 0.1 Å and 0.2 Å. The difference spectra averaged from 450 fs to 550 fs are also plotted to illustrate the rapid bond elongation at times <500 fs. (d) The difference spectrum and estimated excited state spectrum at 100 ps compared with the simulated results using ground state axial bond lengths and a corrin ring expanded 70% of the distance between the ground state ring and the Rbl ring and the axial bonds expanded by 0.05 Å. The experimental data in this panel is reproduced from Ref. 32 copyright 2019, American Chemical Society.

The XANES difference spectrum at the earliest times is dominated by an increase in absorption around 7.73 keV with approximately equal contributions in the *x* and *y*+*z* directions reflecting an expansion of the corrin ring around the cobalt (Figure 12(a)). The expansion is about half as large as the difference between the ground state and Rbl rings, with an average increase in the Co-N distances of ca. 0.043 Å. The red-shift of the XAS edge monitored around 7.72 keV is slightly delayed from the initial excitation, and dominated by *y*+*z* (see Figure 8). The difference spectrum at 300 fs is similar to the difference spectrum at 100 ps, suggesting that the structural distortion is similar (Figure 12(b)). The magnitude of the structural distortion in the excited state is significantly larger at 500 fs, and approximately constant from 500 fs to 1.5 ps, with increased contributions in both the *x* and *y*+*z* directions. The larger *x*-polarized contribution suggests that the expansion of the corrin ring is larger for **B** than for the metastable state **D**. In agreement with

this observation, the *x*-polarized component of the difference spectrum is consistent with the difference between the ground state and Rbl rings as illustrated in Figures 12(c). The average increase in the Co-N_{eq} bonds in the simulation is +0.085 Å (range: +0.074 Å to +0.097 Å). The *y*+*z* component requires a larger axial contribution as well, with a ca. 0.1 Å expansion of the Co-C bond and a ca. 0.2 Å expansion of the Co-N bond providing qualitative agreement with the measurement. While a better model for the ring distortion will be required to refine the axial bond length changes as a function of time delay, it is clear that substantial expansion of both axial bonds is required to account for the magnitude and breadth of the observed difference signal in the **B** state from 500 fs to 1.5 ps.

DISCUSSION

In the experiments presented above, femtosecond to picosecond time-resolved UV-visible absorption, Co K-edge X-ray absorption, and Co Kα, Kβ, and valence-to-core emission, were combined to characterize the excited state dynamics of MeCbl in aqueous solution.

A: τ <200 fs

Excitation of MeCbl in the αβ-band region produces an initial excited state that is primarily corrin-centered (π→π*), although quantum chemical calculations suggest significant involvement of Co 3d character in the occupied orbitals involved in the allowed transitions.[43,47-52] The stimulated emission contribution to the UV-visible transient absorption spectrum (Figure 4) suggests that the lifetime of the initially excited state is ca. 130 fs followed by evolution to a dark state. In the initial state, the Kα and Kβ X-ray emission spectra are broadened slightly (Figure 10), but significant shifts in the emission peaks only develop on a longer time scale suggesting that the net change around the cobalt is relatively small in the bright state.

The valence-to-core X-ray emission and pre-edge X-ray absorption spectra provide more

insight into the initial bright state. In this state, the $1s \rightarrow 3d_{z^2}$ absorption transition is immediately bleached, either because of an increase in the electron density in the $3d_{z^2}$ orbital or because of a decrease in the mixing of this orbital with the Co $4p_z$ orbitals. As illustrated in Figure 13(b), the initial bleach has the full width of the ground state transition, with no evidence for new intensity in other pre-edge transitions in this region. The initial transient in the valence-to-core region is characterized by a decrease in emission on the high-energy side peaking around 7.7061 keV. A comparison of the valence-to-core spectrum of MeCbl with a TD-DFT calculation of the transitions involved in this spectrum is plotted in Figure 12. The dominant transition on the high-energy wing of the emission spectrum is also calculated to be z-polarized, with significant mixing of C_{CH3} and $N_{imidazole}$ $2p_z$ ligand orbitals with the Co $3d_{z^2}/4p_z$ orbital. The initial decrease in emission intensity appears to overlap with this transition.

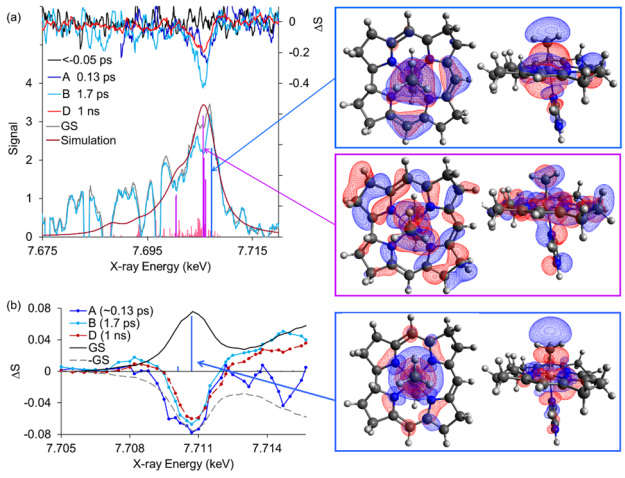

Figure 13. (a) Comparison of the valence-to-core spectrum of MeCbl with a TD-DFT simulation of the transitions involved. The high frequency large fluctuations in the ground state spectrum result from a poor characterization of the detector background. This cancels in the light minus dark difference spectra. The estimated excited state spectrum for species **B** is also plotted to provide an indication of the magnitude of the changes in the emission spectrum. The orbitals making dominant contributions are illustrated to the right. The three transitions around 7.705 keV are polarized in the

corrin ring. The transition at 7.7065 keV is *z*-polarized. (b) Comparison of the X-ray absorption pre-edge transitions of MeCbl with a TD-DFT simulation of the transitions involved.

The exponential model assumed by the global analysis of UV-Visible TA and XES provides useful insights into the excited state dynamics, but careful consideration of the X-ray absorption highlights the inadequacy of such a model (see Figure S6). The initial structural dynamics following photoexcitation can be characterized from the XANES difference spectra in a manner similar to that used previously for AdoCbl,[42] where the signal in each energy region plotted in Figure 9 is fit to a step function convoluted with a Gaussian. An exponential decay is included to account for the longer time scale behavior when necessary. For these fits, the decay was fixed to 1.7 ps, consistent with the optical transient absorption and the time-resolved X-ray emission. The fits are plotted in Figure 14 and the parameters are summarized in Table 1. The time for maximum overlap of the optical and X-ray pulses and the instrument response function (IRF) are set using the earliest and fastest rising transient in the data. This is the bleach of the z-polarized pre-edge transition centered at 7.711 keV. At the other energies, the signal is characterized by a delayed onset and convoluted with a slower Gaussian rise $\sigma_f = \sqrt{\sigma_{IRF}^2 + \sigma_m^2}$, where σ_m is the width corresponding to the intrinsic material response. The data reflect sequential structural evolution of MeCbl on the excited state surface. Ring expansion probed at 7.729 keV may be delayed slightly (~ 30 fs) from the bleach of the pre-edge transition, while the edge shift is delayed ~70 fs from excitation. Rapid axial expansion in MeCbl is consistent with the resonance Raman excitation profile of the Co-C vibration at 505 cm^{-1}.[52] Brunold and coworkers deduce an excited state slope consistent with harmonic displacement > 0.1 Å in the Co-C bond, although the accompanying expansion of the Co-N_{DMB} bond was not evident in the Raman data, perhaps because this stretching motion is distributed over a number of Raman bands.

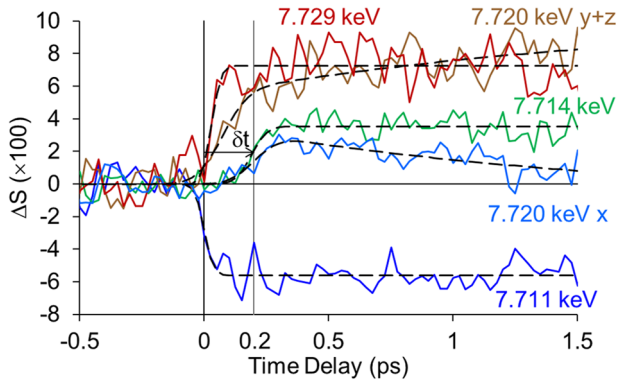

Figure 14. Fit of the XANES difference spectra of MeCbl averaged over select energy regions to a displaced step function convoluted with a Gaussian. The time-displacement from the earliest signal, δt, for the 7.714 keV trace is indicated on the plot. An exponential contribution with τ=1.7 ps is also included for the data around 7.720 keV.

Table 1. Fits of Select Time Traces Following Excitation of MeCbl in Water to a Step Function Delayed by δt and Convoluted with a Gaussian Rise of Width σ_f; σ_m and $\Delta t_m = 2\sqrt{2\ln(2)}\sigma_m$ Represent the Width of the Rise after Deconvolution of the IRF

X-ray energy (keV)	δt (fs)	σ_f (fs)	σ_m (fs)	Δt_m (fs) fwhm
7.711	0	30 ± 4 (IRF)	-	70 (IRF)
7.714	190 ± 10	50 ± 4	40	94
7.720 y+z	70 ± 10	82 ± 4	77	180
7.720 x	200 ± 10	77 ± 4	71	168
7.729	30 ± 10	30 ± 4 (IRF)	-	70 (IRF)

The ~70 fs edge shift for MeCbl is significantly faster than the ~200 fs edge shift observed for AdoCbl.[42] In contrast to MeCbl, there is no strong resonance Raman enhancement of a Co-C stretch in AdoCbl.[53,54] In fact, there is no single clear Co-C vibration in the Raman spectrum of AdoCbl. At least four bands between 420 cm^{-1} and 569 cm^{-1} in the Raman spectrum are sensitive to 5′-$^{12}CH_2/^{13}CH_2$ and/or 5′-CH_2/CD_2 substitution.[53,55] The mode at 569 cm^{-1} involves ribose deformation mixed with the Co-C stretching motion. This appears to be the dominant Co-C stretching mode for AdoCbl.[54] This peak is only weakly enhanced in the resonance Raman

spectrum obtained with 568.2 nm excitation on the red-edge of the αβ-band absorption[53] in contrast to the relatively strong enhancement of the Co-C stretching mode in MeCbl obtained with a similar excitation wavelength.[52] Thus, both the resonance Raman enhancement and tr-XANES suggest that axial elongation begins in the initial Franck-Condon excited state for MeCbl, while for AdoCbl elongation occurs in the dark state after evolution out of the initial excited state.

Combining all of the data; evolution out of the initial excited state occurs on a time scale <190 fs consistent with the ca. 130 fs decay component in the exponential fit to the transient UV-visible and XES spectra. Significant structural evolution occurs in this state, including ring expansion and expansion of the axial bonds. The sequential structural evolution is not well modeled using a sum of exponential components and requires consideration of wavepacket dynamics on the excited state potential energy surface.

B: ~300 fs<τ<~3 ps

The optical absorption spectrum of the dark excited state populated after a couple hundred femtoseconds resembles typical cob(III)alamin species with an αβ-band in the visible centered around 525 nm and a strong γ-band peaking at 340 nm. This spectrum is similar to the relaxed excited state, with the primary difference being increased absorption intensity on the red-edge of the spectrum. Given that the excess energy available to the molecule is larger for 407 nm excitation or 270 nm excitation than for 540 nm, differences in structural relaxation may account for the differences in the UV-visible transient absorption spectra measured using different excitation wavelengths (see FigureS2).

New transitions appear in the pre-edge region for **B**, a weak absorption to the red of the ground state transition and a somewhat stronger absorption to the blue of the ground state transition. The *y*+*z*-polarized transient around 7.714 keV rises sharply, but is delayed by about 190 fs from t=0.

There is no significant *x*-polarized contribution (see Figure 8). It is likely that the increase in intensity in this region represents coherent evolution onto a dark potential surface accompanied by a change in electronic configuration opening a *z*- (or *y*-) polarized transition. The transition observed at ca. 7.709 keV, to the red of the ground state transition is also dominated by a *y*+*z*-polarized contribution, although some *x*-polarized contribution cannot be ruled out. These transitions exhibit a small decay as the population evolves from **B** to **C** to **D**, but the qualitative features are unchanged (Figure 13(b) and Figure S7). The split $1s \rightarrow 3d$ transitions reflect a change in occupancy of Co 3*d* orbitals or in the mixing of 3*d* and 4*p* orbitals.

The VtC emission intensity will be modified both by changes in the occupancy of the Co 3*d* orbitals, and by changes in the overlap of the Co frontier orbitals with the ligand orbitals. Emission near the peak of the spectrum is dominated by in-ring polarized transitions involving the overlap of Co d_{xy}, p_x and p_y orbitals with the equatorial nitrogen atoms (Figure 13(a)). Species **B** is characterized by an increased bleach of the emission and by a shift in the peak of the difference spectrum from 7.7061 keV to 7.7057 keV. The decrease in VtC intensity is consistent with the increase in the cavity around the Co, that is seen in the XANES spectra (~0.08 to 0.10 Å for Co-N_{eq} and Co-C and an even longer expansion of the Co-N_{DMB} bond, See Figure S8).

The large changes in the Kβ and Kα regions are also consistent with significant changes in the electron density and bonding at the Co. In state **B** the Kβ mainline peak broadens and blue shifts by ~0.47 eV from the ground state before recovering to a blue-shift of ~0.27 eV from the ground state. Such a shift is commonly discussed in terms of an increase in spin at the metal or a decrease in covalency of the metal-ligand bonds. In a simplified picture, the metal-centered orbitals are described as linear combinations of metal and ligand orbitals:[56]

$$\psi_d \approx (1-a^2)^{1/2}\varphi_{3d} + a\varphi_L \qquad (4)$$

where *a* represents the amount of ligand character. The position of the Kβ mainline shifts to higher energy as the covalent character decreases. The magnitude of the difference spectrum, and thus of the shift from the ground state (S=0), is larger for the excited states of MeCbl than for the formation of cob(II)alamin (S=1/2). The latter is typically attributed to 3*p*-3*d* spin exchange; however, there is no evidence for intersystem crossing in to a triplet state in photoexcited MeCbl. Our data thus suggest that changes in the covalent interaction of the Co atom with its ligands in the excited electronic states can cause equally large changes in the effective spin at the Co atom. The changes in the Kα emission follow the same trends as the changes in the Kβ region, although they are smaller, consistent with the weaker 2p-3d coupling. The dominant effect in the Kα region is a broadening of the peaks, with only a small blue shift in the $K\alpha_1$ emission of ~0.1 to 0.15 eV in all excited states. The magnitude of the broadening decreases over the first two picoseconds, but significant changes remain in the relaxed excited states **C/D**.

Combining all of the data; the excited state **B** is characterized by a change in the electronic distribution around the central cobalt atom and by significant expansion of the cavity around the cobalt atom (Δr ~0.1 Å). The cavity collapses somewhat around the cobalt as the molecule relaxes in the excited state, but the expansion remains ≥0.05 Å.

C/D: τ >~5 ps

The excited state behavior of MeCbl is distinct from that of other alkylcobalamins. We have measured bond homolysis yields for a range of alkylcobalamins, and find yields approaching 100% on time scales of 100 ± 50 ps in all cases except MeCbl.[23,29,57] The ultimate quantum yields for Co-C homolysis can be variable, depending on the competition between cage escape and geminate recombination rate,[57,58] but the initial yield of radical pairs is high. In contrast, optical excitation of MeCbl in the visible absorption band results in population of a metastable excited state with a

ca. 1 ns lifetime in water and a ca. 2.4 ns lifetime in ethylene glycol. The yield for bond homolysis from this state is ≤15% in water and <15% in ethylene glycol. The majority of the population returns to the ground state of MeCbl. The steady state quantum yield is controlled by branching between bond dissociation and internal conversion to the ground state rather than by the probability of geminate recombination.

The behavior of the photoreceptor CarH resembles that of MeCbl, with visible excitation resulting in formation of a metastable excited state having a lifetime of several nanoseconds.[17] This behavior is distinct from that of AdoCbl either free in solution or bound to proteins,[15,18,19] demonstrating that some aspect of the CarH site is able to modify AdoCbl so that it has behavior that is otherwise seen only for MeCbl. The UV-visible spectrum of the CarH excited state and the magnitude of its XANES difference spectrum are similar to those of MeCbl,[17,21] suggesting that the structural and electronic changes may be similar. In contrast, both the transient absorption and the XANES differences following excitation of AdoCbl in water are distinctly different from those seen in either CarH or MeCbl. The evolution of the optical spectrum of AdoCbl in water is compared with MeCbl in Figure 5. In contrast to the modest changes observed for MeCbl and for AdoCbl bound to CarH, significant evolution is observed for AdoCbl. Here the X-ray measurements on MeCbl may provide some additional insight. The changes in the XANES and XES spectra for the metastable state **D** are consistent with contraction of the Co-ligand bond lengths from the point of maximum distortion, but the ring remains expanded and the transients support assignment to an excited state with increased electron density on the cobalt. A more complete analysis of the structural changes as a function of time will require the development of more sophisticated methods to optimize the structure and compare simulations with the experimental X-ray absorption and emission spectra.

Bond Dissociation

Although formation of cob(II)alamin is a secondary channel following excitation of MeCbl, it is of interest to compare the cob(II)alamin form with the relaxed excited state **D**. The XANES difference spectrum for the formation of cob(II)alamin was discussed previously.[32,46] Briefly, the dominant change is axial, reflecting loss of the methyl ligand and a ca. 0.08 Å contraction of the Co-N_{DMB} bond. The ring changes are smaller than for the excited electronic states; and increase of ca. 0.03 Å in the Co-N_{corrin} bonds provides qualitative agreement with the measured spectrum.[46] This is approximately half of the magnitude of the change required to model the metastable excited state **D**. The XES difference spectra provide additional insight into the nature of the cob(II)alamin species. The difference spectrum for formation of **D** is asymmetric reflecting a blue shift of the Kβ mainline peak, accompanied by some broadening and a small increase in emission in the region generally attributed to Kβ′, indicating increased spin density on the cobalt. In contrast, the difference spectrum for formation of cob(II)alamin is symmetric, with little, if any, increase in emission in the Kβ′ region despite the explicit formation of a radical species with a low spin Co (S=1/2) and spin density localized in a Co d_{z^2} orbital.[59-61] In this case, electronic excitation causes a bigger change in the XES than bond dissociation and a change in the formal oxidation state.

CONCLUSIONS

Time-resolved XAS of MeCbl in the pre-edge and XANES regions has been combined with time-resolved XES in the $K\alpha_{1,2}$, $K\beta_{1,3}$, and valence-to-core regions and with transient UV-visible spectroscopy spanning the range from 290 nm to 730 nm. The combinations of methods provide a powerful tool to probe the femtosecond and picosecond electronic and structural dynamics on photoactive transition metal complexes. Polarized XANES difference spectra allow characterization of sequential structural evolution. The initial dynamics involve equatorial

expansion of the corrin ring around the central cobalt coupled with elongation of the Co-C bond in the Franck-Condon allowed fluorescent excited state. This is consistent with resonance Raman excitation profile where both Co-CH_3 and corrin ring stretching motions show significant enhancement.[52] Time-resolved XES, especially in the Kβ and VtC regions, along with polarized XANES suggests that the state that is populated as the molecule moves into the initial dark state is characterized by a prompt change in electronic configuration and coherent expansion of both axial and equatorial bonds, with the elongation slightly overshooting the excited state minimum before the molecule relaxes into a metastable state **D** having a nanosecond lifetime. The metastable state is characterized by expansion around the central Co of ~0.05 Å and increased electron density on the Co ion approaching which might be expected for a 6-coordinate Co^{2+} with a corrin π-cation.

The primary difference between the XES spectra of the MeCbl ground state and the cob(II)alamin product is a broadening of the $K\beta_{1,3}$ emission line. In contrast, the excited state is characterized by a blue shift of this emission line leading to an asymmetric difference spectrum. Surprisingly, the difference between the 6-coordinate excited state and the ground state is significantly larger than the difference between 6-coordinate MeCbl and 5-coordinate cob(II)alamin. This suggests the need for some caution when using ground state spectra of stable molecules to identify transient excited state species.

The spectroscopic similarity between the metastable state formed from MeCbl excitation and that formed following excitation of CarH suggests that MeCbl – an outlier among alkyl cobalamins because of its unique behavior – may be an excellent analog for CarH.

SUPPORTING INFORMATION

A pdf file including additional transient absorption spectra, global analysis of X-ray emission spectra, comparison of fits to the X-ray absorption pre-edge region, and simulations of the valence-

to-core emission spectrum is available.

DATA AVAILABILITY

The processed data used to produce the figures shown in the manuscript and supporting material are available from DeepBlue (DOI: 10.7302/9ycc-t185). Details of the beamtime proposals and data recorded for the experiment at the European XFEL are available at doi:10.22003/XFEL.EU-DATA-002715-00 and doi:10.22003/XFEL.EU-DATA-003079-00.

ACKNOWLEDGEMENTS

This work was supported by grants from the National Science Foundation NSF-CHE 1836435, NSF-CHE 2154157 to RJS. Partial support for RAM came from NIH grant P41GM139687. Use of the Linac Coherent Light Source (LCLS), SLAC National Accelerator Laboratory, is supported by the U.S. Department of Energy, Office of Science, Office of Basic Energy Sciences under Contract No. DE-AC02-76SF00515. Use of the Stanford Synchrotron Radiation Lightsource, SLAC National Accelerator Laboratory, is supported by the U.S. Department of Energy, Office of Science, Office of Basic Energy Sciences under Contract No. DE-AC02-76SF00515. We would like to thank the staff for their assistance. We acknowledge European XFEL in Schenefeld, Germany, for provision of X-ray free-electron laser beamtime at Scientific Instrument FXE (Femtosecond X-Ray Experiments) and would like to thank the staff for their assistance.

REFERENCES

(1) Mascarenhas, R.; Gouda, H.; Ruetz, M.; Banerjee, R., Human B12-dependent enzymes: Methionine synthase and Methylmalonyl-CoA mutase In *Methods in Enzymology*; Marsh, E. N. G., Ed.; Academic Press: 2022; Vol. 668, p 309-326, 10.1016/bs.mie.2021.12.012

(2) Padmanabhan, S.; Jost, M.; Drennan, C. L.; Elias-Arnanz, M., A new facet of vitamin B_{12}: Gene regulation by cobalamin-based photoreceptors. *Annu. Rev. Biochem.* **2017**, *86*, 485-514, 10.1146/annurev-biochem-061516-044500.

(3) Giedyk, M.; Goliszewska, K.; Gryko, D., Vitamin B_{12} catalysed reactions. *Chem. Soc. Rev.* **2015**, *44*, 3391-3404, 10.1039/c5cs00165j.

(4) Marques, H. M., The inorganic chemistry of the cobalt corrinoids – an update. *J. Inorg. Biochem.* **2023**, *242*, 112154, 10.1016/j.jinorgbio.2023.112154.

(5) Padmanabhan, S.; Perez-Castano, R.; Elias-Arnanz, M., B-12-based photoreceptors: from structure and function to applications in optogenetics and synthetic biology. *Curr. Opin. Struct. Biol.* **2019**, *57*, 47-55, 10.1016/j.sbi.2019.01.020.

(6) Miller, N. A.; Wiley, T. E.; Spears, K. G.; Ruetz, M.; Kieninger, C.; Kräutler, B.; Sension, R. J., Toward the design of photoresponsive conditional antivitamins B_{12}: A transient absorption study of an arylcobalamin and an alkynylcobalamin. *J. Am. Chem. Soc.* **2016**, *138*, 14250-14256,

(7) Welfare, J. G.; Mortelliti, M. J.; McGlade, C. A.; Hartman, T. W.; Dempsey, J. L.; Lawrence, D. S., Assessment of Photoreleasable Linkers and Light-Capturing Antennas on a Photoresponsive Cobalamin Scaffold. *J. Org. Chem.* **2022**, *87*, 5076-5084, 10.1021/acs.joc.1c02931.

(8) Rodgers, Z. L.; Shell, T. A.; Brugh, A. M.; Nowotarski, H. L.; Forbes, M. D. E.; Lawrence, D. S., Fluorophore Assisted Photolysis of Thiolato-Cob(III)alamins. *Inorg. Chem.* **2016**, *55*, 1962-1969, 10.1021/acs.inorgchem.5b02036.

(9) Shell, T. A.; Lawrence, D. S., Vitamin B_{12}: A tunable, long wavelength, light-responsive platform for launching therapeutic agents. *Acc. Chem. Res.* **2015**, *48*, 2866-2874, 10.1021/acs.accounts.5b00331.

(10) Bam, R.; Pollatos, A. S.; Moser, A. J.; West, J. G., Mild olefin formation via bio-inspired vitamin B12 photocatalysis. *Chem. Sci.* **2021**, *12*, 1736-1744, 10.1039/D0SC05925K.

(11) Funk, B. E.; Pauze, M.; Lu, Y.-C.; Moser, A. J.; Wolf, G.; West, J. G., Vitamin B12 and hydrogen atom transfer cooperative catalysis as a hydride nucleophile mimic in epoxide ring opening. *Cell Reports Physical Science* **2023**, *4*, 101372, 10.1016/j.xcrp.2023.101372.

(12) Peng, J.; Tang, K. C.; McLoughlin, K.; Yang, Y.; Forgach, D.; Sension, R. J., Ultrafast Excited-State Dynamics and Photolysis in Base-Off B-12 Coenzymes and Analogues: Absence of the trans-Nitrogenous Ligand Opens a Channel for Rapid Nonradiative Decay. *J. Phys. Chem. B* **2010**, *114*, 12398-12405, 10.1021/jp104641u.

(13) Al Mamun, A.; Toda, M. J.; Lodowski, P.; Kozlowski, P. M., Photolytic Cleavage of Co-C Bond in Coenzyme B-12-Dependent Glutamate Mutase. *J. Phys. Chem. B* **2019**, *123*, 2585-2598, 10.1021/acs.jpcb.8b07547.

(14) Toda, M. J.; Lodowski, P.; Al Mamun, A.; Jaworska, M.; Kozlowski, P. M., Photolytic properties of the biologically active forms of vitamin B_{12}. *Coord. Chem. Rev.* **2019**, *385*, 20-43, 10.1016/j.ccr.2018.12.017.

(15) Harris, D. A.; Stickrath, A. B.; Carroll, E. C.; Sension, R. J., Influence of environment on the electronic structure of cob(III)alamins: Time-resolved absorption studies of the S_1 state spectrum and dynamics. *J. Am. Chem. Soc.* **2007**, *129*, 7578-7585, 10.1021/ja066197y.

(16) Wiley, T. E.; Miller, N. A.; Miller, W. R.; Sofferman, D. L.; Lodowski, P.; Toda, M. J.; Jaworska, M.; Kozlowski, P. M.; Sension, R. J., Off to the races: Comparison of excited state

dynamics in vitamin B_{12} derivatives hydroxocobalamin and aquocobalamin. *J. Phys. Chem. A* **2018**, *122*, 6693-6703, 10.1021/acs.jpca.8b06103.

(17) Miller, N. A.; Kaneshiro, A. K.; Konar, A.; Alonso-Mori, R.; Britz, A.; Deb, A.; Glownia, J. M.; Koralek, J. D.; Mallik, L.; Meadows, J. H. et al.;, The Photoactive Excited State of the B12-Based Photoreceptor CarH. *J. Phys. Chem. B* **2020**, *124*, 10732−10738, 10.1021/acs.jpcb.0c09428.

(18) Sension, R. J.; Harris, D. A.; Stickrath, A.; Cole, A. G.; Fox, C. C.; Marsh, E. N. G., Time-resolved measurements of the photolysis and recombination of adenosylcobalamin bound to glutamate mutase. *J. Phys. Chem. B* **2005**, *109*, 18146-18152, 10.1021/jp052492d.

(19) Sension, R. J.; Cole, A. G.; Harris, A. D.; Fox, C. C.; Woodbury, N. W.; Lin, S.; Marsh, E. N. G., Photolysis and recombination of adenosylcobalamin bound to glutamate mutase. *J. Am. Chem. Soc.* **2004**, *126*, 1598-1599, 10.1021/ja0396910.

(20) Jones, A. R., The photochemistry and photobiology of vitamin B_{12}. *Photochem. Photobiol. Sci.* **2017**, *16*, 820-834, 10.1039/c7pp00054e.

(21) Kutta, R. J.; Hardman, S. J. O.; Johannissen, L. O.; Bellina, B.; Messiha, H. L.; Ortiz-Guerrero, J. M.; Elias-Arnanz, M.; Padmanabhan, S.; Barran, P.; Scrutton, N. S. et al.;, The photochemical mechanism of a B_{12}-dependent photoreceptor protein. *Nat. Commun.* **2015**, *6*, 7907, 10.1038/ncomms8907.

(22) Walker II, L. A.; Shiang, J. J.; Anderson, N. A.; Pullen, S. H.; Sension, R. J., Time-resolved spectroscopic studies of B_{12} coenzymes: The photolysis and geminate recombination of adenosylcobalamin. *J. Am. Chem. Soc.* **1998**, *120*, 7286-7292,

(23) Sension, R. J.; Harris, D. A.; Cole, A. G., Time-resolved spectroscopic studies of B_{12} coenzymes: A comparison of the influence of solvent on the primary photolysis mechanism and geminate recombination of methyl-, ethyl-, n-propyl-, and 5'-deoxyadenosylcobalamin. *J. Phys.*

Chem. B **2005**, *109*, 21954-21962, 10.1021/jp053202w.

(24) Yoder, L. M.; Cole, A. G.; Walker II, L. A.; Sension, R. J., Time-resolved spectroscopic studies of B_{12} coenzymes: Influence of solvent on the photolysis of adenosylcobalamin. *J. Phys. Chem. B* **2001**, *105*, 12180-12188, 10.1021/jp012157z.

(25) Jost, M.; Simpson, J. H.; Drennan, C. L., The transcription factor CarH safeguards use of adenosylcobalamin as a light sensor by altering the photolysis products. *Biochemistry* **2015**, *54*, 3231-3234, 10.1021/acs.biochem.5b00416.

(26) Shiang, J. J.; Walker II, L. A.; Anderson, N. A.; Cole, A. G.; Sension, R. J., Time-resolved spectroscopic studies of B_{12} coenzymes: The photolysis of methylcobalamin is wavelength dependent. *J. Phys. Chem. B* **1999**, *103*, 10532-10539, 10.1021/jp992358r.

(27) Walker II, L. A.; Jarrett, J. T.; Anderson, N. A.; Pullen, S. H.; Matthews, R. G.; Sension, R. J., Time-resolved spectroscopic studies of B_{12} coenzymes: The identification of a metastable cob(III)alamin photoproduct in the photolysis of methylcobalamin. *J. Am. Chem. Soc.* **1998**, *120*, 3597-3603, 10.1021/ja974024q.

(28) Shiang, J. J.; Cole, A. G.; Sension, R. J.; Hang, K.; Weng, Y.; Trommel, J. S.; Marzilli, L. G.; Lian, T., Ultrafast Excited-State Dynamics in Vitamin B_{12} and Related Cob(III)Alamins. *J. Am. Chem. Soc.* **2006**, *128*, 801-808, 10.1021/ja054374+.

(29) Cole, A. G.; Yoder, L. M.; Shiang, J. J.; Anderson, N. A.; Walker II, L. A.; Banaszak Holl, M. M.; Sension, R. J., Time-resolved spectroscopic studies of B_{12} coenzymes: A comparison of the primary photolysis mechanism in methyl-, ethyl-, n-propyl-, and 5'-deoxyadenosylcobalamin. *J. Am. Chem. Soc.* **2002**, *124*, 434-441, 10.1021/ja011628s.

(30) Chollet, M.; Alonso-Mori, R.; Cammarata, M.; Damiani, D.; Defever, J.; Delor, J. T.; Feng, Y. P.; Glownia, J. M.; Langton, J. B.; Nelson, S. et al.;, The X-ray pump-probe instrument at the

Linac Coherent Light Source. *J. Synchrot. Radiat.* **2015**, *22*, 503-507, 10.1107/S1600577515005135.

(31) Antolini, C.; Sosa Alfaro, V.; Reinhard, M.; Chatterjee, G.; Ribson, R.; Sokaras, D.; Gee, L.; Sato, T.; Kramer, P. L.; Raj, S. L. et al.;, The Liquid Jet Endstation for Hard X-ray Scattering and Spectroscopy at the Linac Coherent Light Source. *Molecules* **2024**, *29*, 2323, 10.3390/molecules29102323.

(32) Michocki, L. B.; Miller, N. A.; Alonso-Mori, R.; Britz, A.; Deb, A.; Glownia, J. M.; Kaneshiro, A. K.; Konar, A.; Meadows, J. H.; Sofferman, D. L. et al.;, Probing the excited state of methylcobalamin using polarized time-resolved X-ray absorption spectroscopy. *J. Phys. Chem. B* **2019**, *123*, 6042-6048, 10.1021/acs.jpcb.9b05854.

(33) Khakhulin, D.; Otte, F.; Biednov, M.; Bömer, C.; Choi, T.-K.; Diez, M.; Galler, A.; Jiang, Y.; Kubicek, K.; Lima, F. A. et al.;, Ultrafast X-ray Photochemistry at European XFEL: Capabilities of the Femtosecond X-ray Experiments (FXE) Instrument. *Applied Sciences* **2020**, *10*, 995, 10.3390/app10030995.

(34) Galler, A.; Gawelda, W.; Biednov, M.; Bomer, C.; Britz, A.; Brockhauser, S.; Choi, T.-K.; Diez, M.; Frankenberger, P.; French, M. et al.;, Scientific instrument Femtosecond X-ray Experiments (FXE): instrumentation and baseline experimental capabilities. *J. Synchrot. Radiat.* **2019**, *26*, 1432-1447, 10.1107/S1600577519006647.

(35) Decking, W.; Abeghyan, S.; Abramian, P.; Abramsky, A.; Aguirre, A.; Albrecht, C.; Alou, P.; Altarelli, M.; Altmann, P.; Amyan, K. et al.;, A MHz-repetition-rate hard X-ray free-electron laser driven by a superconducting linear accelerator. *Nature Photonics* **2020**, *14*, 391-397, 10.1038/s41566-020-0607-z.

(36) Lima, F. A.; Otte, F.; Vakili, M.; Ardana-Lamas, F.; Biednov, M.; Dall'Antonia, F.;

Frankenberger, P.; Gawelda, W.; Gelisio, L.; Han, H. et al.;, Experimental capabilities for liquid jet samples at sub-MHz rates at the FXE Instrument at European XFEL. *J. Synchrot. Radiat.* **2023**, *30*, 1168-1182, 10.1107/S1600577523008159.

(37) Bunau, O.; Joly, Y., Self-consistent aspects of X-ray absorption calculations. *J. Phys. Condens. Matter* **2009**, *21*, 345501, 10.1088/0953-8984/21/34/345501.

(38) Joly, Y., X-ray absorption near-edge structure calculations beyond the muffin-tin approximation. *Phys. Rev. B* **2001**, *63*, 125120, 10.1103/PhysRevB.63.125120.

(39) Neese, F., Software update: The ORCA program system—Version 5.0. *WIREs Comput. Mol. Sci.* **2022**, *12*, e1606, 10.1002/wcms.1606.

(40) Neese, F., The ORCA program system. *WIREs Comput. Mol. Sci.* **2012**, *2*, 73-78, 10.1002/wcms.81.

(41) Snellenburg, J. J.; Laptenok, S.; Seger, R.; Mullen, K. M.; van Stokkum, I. H. M., Glotaran: A Java-based graphical user interface for the R package TIMP. *J. Stat. Soft.* **2012**, *49*, 1-22, 10.18637/jss.v049.i03.

(42) Miller, N. A.; Michocki, L. B.; Konar, A.; Alonso-Mori, R.; Deb, A.; Glownia, J. M.; Sofferman, D. L.; Song, S.; Kozlowski, P. M.; Kubarych, K. J. et al.;, Ultrafast XANES monitors sequential structural evolution in photoexcited coenzyme B_{12}. *J. Phys. Chem. B* **2020**, *124*, 199-209, 10.1021/acs.jpcb.9b09286.

(43) Lodowski, P.; Jaworska, M.; Andruniow, T.; Garabato, B. D.; Kozlowski, P. M., Mechanism of Co−C bond photolysis in the base-on form of methylcobalamin. *J. Phys. Chem. A* **2014**, *118*, 11718-11734,

(44) Widner, F. J.; Lawrence, A. D.; Deery, E.; Heldt, D.; Frank, S.; Gruber, K.; Wurst, K.; Warren, M. J.; Krautler, B., Total Synthesis, Structure, and Biological Activity of

Adenosylrhodibalamin, the Non-Natural Rhodium Homologue of Coenzyme B_{12}. *Angew. Chem., Int. Ed.* **2016**, *55*, 11281-11286, 10.1002/anie.201603738.

(45) Hannibal, L.; Smith, C. A.; Smith, J. A.; Axhemi, A.; Miller, A.; Wang, S.; Brasch, N. E.; Jacobsen, D. W., High Resolution Crystal Structure of the Methylcobalamin Analogues Ethylcobalamin and Butylcobalamin by X-ray Synchrotron Diffraction. *Inorg. Chem.* **2009**, *48*, 6615-6622, 10.1021/ic900590p.

(46) Chung, T.; McClain, T. P.; Alonso-Mori, R.; Chollet, M.; Deb, A.; Garcia-Esparza, A.; Huang Ze En, J.; Lamb, R. M.; Michocki, L. B.; Reinhard, M. et al.;, Ultrafast X-ray spectroscopy reveals excited state dynamics of B_{12} coenzymes controlled by the axial base. *J. Phys. Chem. B* **2024**, *128*, 1428-1437, 10.1021/acs.jpcb.3c07779.

(47) Kornobis, K.; Kumar, N.; Lodowski, P.; Jaworska, M.; Piecuch, P.; Lutz, J. J.; Wong, B. M.; Kozlowski, P. M., Electronic structure of the S1 state in methylcobalamin: Insight from CASSCF/MC-XQDPT2, EOM-CCSD, and TD-DFT calculations. *J. Comp. Chem.* **2013**, *34*, 987-1004,

(48) Lodowski, P.; Jaworska, M.; Andruniow, T.; Kumar, M.; Kozlowski, P. M., Photodissociation of Co-C bond in methyl- and ethylcobalamin: An insight from TD-DFT calculations. *J. Phys. Chem. B* **2009**, *113*, 6898-6909, 10.1021/jp810223h.

(49) Andruniów, T.; Jaworska, M.; Lodowski, P.; Zgierski, M. Z.; Dreos, R.; Randaccio, L.; Kozlowski, P. M., Time-dependent density functional theory study of cobalt corrinoids: Electronically excited states of methylcobalamin. *J. Chem. Phys.* **2008**, *129*, 085101,

(50) Lodowski, P.; Jaworska, M.; Garabato, B. D.; Kozlowski, P. M., Mechanism of Co–C Bond Photolysis in Methylcobalamin: Influence of Axial Base. *J. Phys. Chem. A* **2015**, *119*, 3913-3928, 10.1021/jp5120674.

(51) Elmendorf, L. D.; Brunold, T. C., Electronic structure studies of free and enzyme-bound B-12 species by magnetic circular dichroism and complementary spectroscopic techniques In *Methods in Enzymology*; Marsh, E. N. G., Ed. 2022; Vol. 669, p 333-365, 10.1016/bs.mie.2022.02.002

(52) Stich, T. A.; Brooks, A. J.; Buan, N. R.; Brunold, T. C., Spectroscopic and computational studies of Co^{3+}-corrinoids: Spectral and electronic properties of the B_{12} cofactors and biologically relevant precursors. *J. Am. Chem. Soc.* **2003**, *125*, 5897-5914, 10.1021/ja029328d.

(53) Dong, S.; Padmakumar, R.; Maiti, N.; Banerjee, R.; Spiro, T. G., Resonance Raman Spectra Show That Coenzyme B12 Binding to Methylmalonyl-Coenzyme A Mutase Changes the Corrin Ring Conformation but Leaves the Co-C Bond Essentially Unaffected. *J. Am. Chem. Soc.* **1998**, *120*, 9947-9948,

(54) Kozlowski, P. M.; Andruniow, T.; Jarzecki, A. A.; Zgierski, M. Z.; Spiro, T. G., DFT analysis of Co-alkyl and Co-adenosyl vibrational modes in B_{12}-cofactors. *Inorg. Chem.* **2006**, *45*, 5585-5590, 10.1021/ic052069j.

(55) Dong, S.; Padmakumar, R.; Banerjee, R.; Spiro, T. G., Co-C Bond Activation in B12-Dependent Enzymes: Cryogenic Resonance Raman Studies of Methylmalonyl-Coenzyme A Mutase. *J. Am. Chem. Soc.* **1999**, *121*, 7063-7070,

(56) Pollock, C. J.; Delgado-Jaime, M. U.; Atanasov, M.; Neese, F.; DeBeer, S., Kβ Mainline X-ray Emission Spectroscopy as an Experimental Probe of Metal–Ligand Covalency. *J. Am. Chem. Soc.* **2014**, *136*, 9453-9463, 10.1021/ja504182n.

(57) Stickrath, A.; Carroll, E. C.; Dai, X.; Harris, D. A.; Rury, A.; Smith, B.; Tang, K.-C.; Wert, J.; Sension, R. J., Solvent-dependent cage dynamics of small nonpolar radicals: Lessons from the photodissociation and geminate recombination of alkylcobalamins. *J. Phys. Chem. A* **2009**, *113*,

8513–8522,

(58) Taylor, R. T.; Smucker, L.; Hanna, M. L.; Gill, J., Aerobic photolysis of alkylcobalamins: Quantum yields and light-action spectra. *Arch. Biochem. Biophys.* **1973**, *156*, 521-533, 10.1016/0003-9861(73)90301-9.

(59) Demissie, T. B.; Repisky, M.; Liu, H.; Ruud, K.; Kozlowski, P. M., Cob(II)alamin: Relativistic DFT analysis of the EPR parameters. *J. Chem. Theory Comput.* **2014**, *10*, 2125-2136, 10.1021/ct400769t.

(60) Harmer, J.; Van Doorslaer, S.; Gromov, I.; Schweiger, A., Corrin nitrogens and remote dimethylbenzimidazole nitrogen interactions in Cob(II)alamin studied with HYSCORE at X- and Q-band. *Chem. Phys. Lett.* **2002**, *358*, 8-16, 10.1016/S0009-2614(02)00521-3.

(61) Joerin, E.; Schweiger, A.; Guenthard, H. H., Single-crystal EPR of the oxygen-17-enriched dioxygen adduct of vitamin B12r: reversible oxygen bonding, electronic and geometric structure and molecular dynamics. *J. Am. Chem. Soc.* **1983**, *105*, 4277-4286, 10.1021/ja00351a027.